Geophys. J. Int. (2000) **142,** 283–299

The 1994 Sefidabeh earthquakes in eastern Iran: blind thrusting and bedding-plane slip on a growing anticline, and active tectonics of the Sistan suture zone

M. Berberian,[1] J. A. Jackson,[2] M. Qorashi,[3] M. Talebian,[3] M. Khatib[4] and K. Priestley[2]

[1] *Najarian Associates, Suite E, One Industrial Way West, Eatontown,* NJ 07724-2255, *USA. E-mail: berberian@najarian.com*
[2] *University of Cambridge, Department of Earth Sciences, Bullard Laboratories, Madingley Road, Cambridge,* CB3 OEZ, *UK. E-mails: jackson@esc.cam.ac.uk; priestley@esc.cam.ac.uk*
[3] *Geological Survey of Iran,* PO Box 13185-1494, *Tehran, Iran. E-mail: seismotec@www.dci.co.ir*
[4] *Department of Geology, Birjand University,* PO Box 79, *Birjand, Iran*

Accepted 2000 February 29. Received 2000 February 21; in original form 1999 October 7

SUMMARY

In 1994 a sequence of five earthquakes with M_w 5.5–6.2 occurred in the Sistan belt of eastern Iran, all of them involving motion on blind thrusts with centroid depths of 5–10 km. Coseismic ruptures at the surface involved bedding-plane slip on a growing hanging-wall anticline displaying geomorphological evidence of uplift and lateral propagation. The 1994 earthquakes were associated with a NW-trending thrust system that splays off the northern termination of a major N–S right-lateral strike-slip fault. Elevation changes along the anticline ridge suggest that displacement on the underlying thrust dies out to the NW, away from its intersection with the strike-slip fault. This is a common fault configuration in eastern Iran and accommodates oblique NE–SW shortening across the N–S deforming zone, probably by anticlockwise rotations about a vertical axis. This style of fault kinematics may be transitional to a more evolved state that involves partitioning of the strike-slip and convergent motion onto separate subparallel faults.

Key words: active tectonics, bedding-plane slip, blind thrusting, earthquakes, eastern Iran.

1 INTRODUCTION

In February 1994 a sequence of four earthquakes with magnitudes (M_s) 5.5–6.1 occurred in the space of a week in a remote area of eastern Iran. Although minor surface ruptures accompanied these earthquakes, they all involved blind thrust faulting beneath a growing anticline ridge. There is considerable interest in blind thrust and reverse faults, particularly following earthquakes on such structures in California at Coalinga (1983), Whittier Narrows (1987) and Northridge (1994). One controversial issue is whether the relatively steep reverse or thrust faults in the upper seismogenic crust flatten at depth into aseismic, subhorizontal ductile shear zones in the lower crust, to produce an overall geometry analogous to the ramp-and-flat style familiar at shallower levels in fold-and-thrust belts (e.g. Namson & Davies 1988; Shaw & Suppe 1994), or whether they continue into the lower crust at a relatively steep dip (Yeats 1993). This issue has implications for palinspastic reconstructions and for calculating shortening rates from surface deformation (e.g Yeats *et al.* 1997). The other important issue is recognizing these structures before they move, which is essential for both tectonic and seismic hazard evaluation (e.g. Bullard & Lettis 1993; Lettis *et al.* 1997). In California, where blind thrusting earthquakes have occurred in oil-producing areas, there are subsurface geological data available to help. In other places we are necessarily dependent on geomorphological indicators, which are a focus of this paper.

The 1994 Sefidabeh earthquakes were associated with clear geomorphological features, superbly preserved and exposed in the desert climate of eastern Iran. They therefore offer an opportunity to combine seismological and geomorphological observations to see how the surface deformation develops in response to continued motion on the blind thrusts at depth. As in California, these active thrusts occur adjacent to active strike-slip faults, thus raising the question of how these fault types interact and contribute to the regional deformation.

2 GEOLOGICAL AND TECTONIC SETTING

2.1 Topography

The Sefidabeh area is located in the central, narrowest, part of the Sistan ranges, which trend N–S along the border between Iran and Afghanistan (Figs 1 and 2), separating the Dasht-e-Lut (*lit.* 'barren desert') in the west from the Dasht-e-Margo (*lit.* 'desert of death') in the east. The highest point in the area

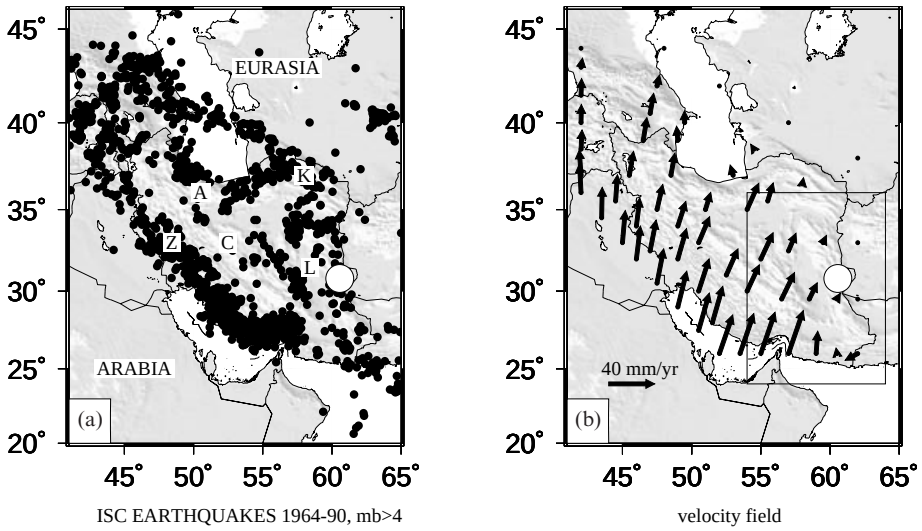

Figure 1. (a) Seismicity of Iran 1964–1990. Note how the cut-off in seismicity follows the NE and E borders of Iran. The Zagros is marked by Z, the Alborz by A, the Kopeh Dagh by K, the relatively aseismic central Iran block by C and the Lut block by L. The 1994 Sefidabeh epicentral region is marked with a white circle on both maps. (b) A velocity field for Iran showing how the NNE motion of Arabia relative to Asia is absorbed in Iran. The distribution of velocities within Iran is estimated from the spatial variation in the style of strain rates indicated by earthquakes (from Jackson *et al.* 1995). Note the expected right-lateral shear and shortening along the eastern border of Iran. The boxed region is the area shown in Fig. 2(a).

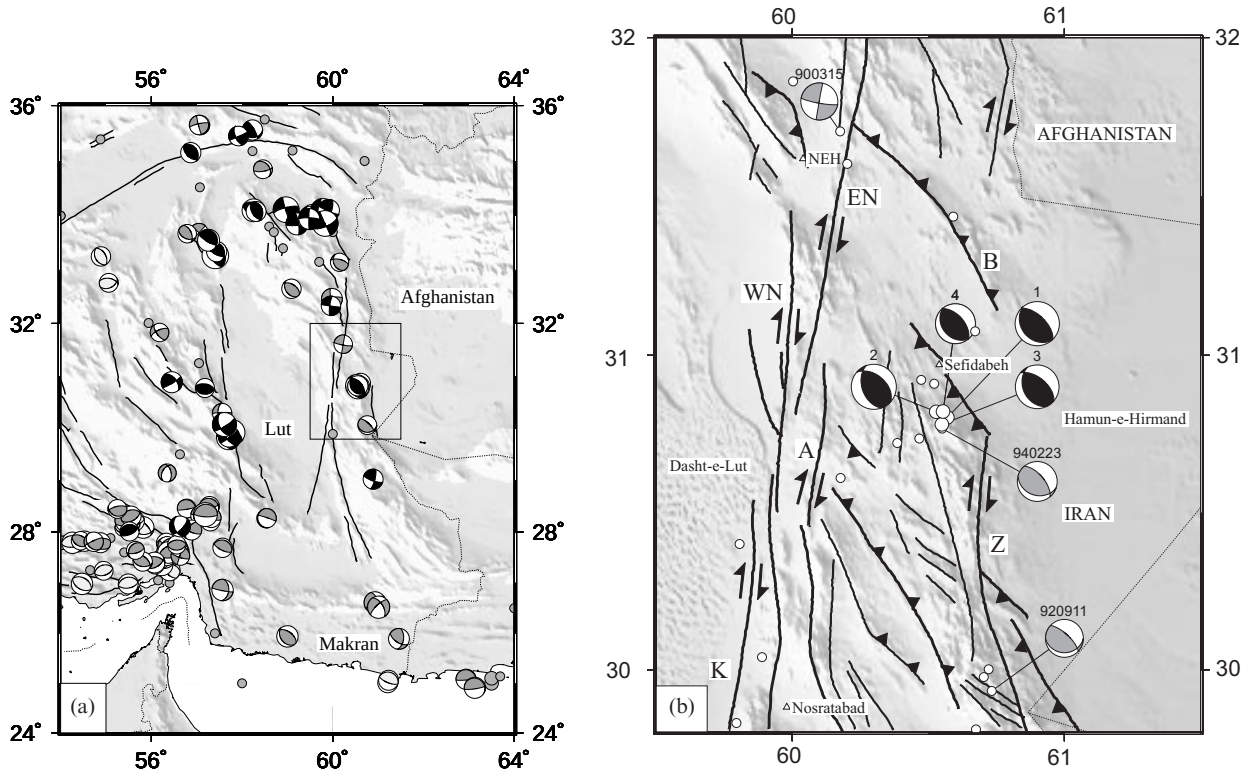

Figure 2. (a) Regional summary map of faults and shallow earthquake focal mechanisms. Mechanisms constrained by body wave inversion (various sources) are in black, dark grey spheres are Harvard CMT solutions, and light grey spheres are first-motion fault plane solutions from Jackson & McKenzie (1984). Grey circles are epicentres of 1900–1963 earthquakes with $M_s \geq 5.7$. Subcrustal earthquakes associated with the Makran subduction zone have been removed. Faults are from Berberian & Yeats (1999). The boxed region is the area of Fig. 2(b). (b) Summary map of the faulting, topography and focal mechanisms in the southern part of the Sistan suture zone. Large white circles and their accompanying black focal spheres marked 1–4 are the locations and mechanisms of the four main earthquakes in the Sefidabeh sequence, whose source parameters are determined in this paper. Grey focal spheres are additional Harvard CMT solutions. Small white circles are other earthquakes located by Engdahl *et al.* (1998) in the period 1964–1995. The pattern of active faults is marked by solid lines: all of those trending N–S are right-lateral strike-slip faults, and those trending NW–SE are thrusts or reverse faults. The Kahurak Fault is marked K, the West and East Neh faults by WN and EN, the Zahedan Fault by Z, the Asagi Fault by A and the Bandan Fault by B.

is Palang Kuh (+2029 m), about 25 km SSE of Sefidabeh, and the lowest (+471 m) is on the fringes of the Hamun-e-Hirmand (*lit.* 'watery') depression 50 km to the east. Sefidabeh itself lies at the foot of an asymmetric NW-trending ridge, steep on its NE side and rising 100–200 m above the Sistan plain near the village (Figs 3 and 4), but decreasing in height along strike to the NW. The region has a low annual rainfall and is barren, inhospitable and sparsely populated.

2.2 Geological setting

The 1994 epicentral region lies in the eastern part of the Sistan 'flysch and coloured melange belt', which is a deformed forearc basin recording the destruction of an arm of the Neo-Tethys during Senonian–Palaeocene times and consequent collision of the Afghan (in the east) and Lut (in the west) cratonic blocks (Camp & Griffis 1982; Tirrul *et al.* 1983). It consists of volcanic, volcaniclastic and flysch deposits, and onlaps the western margin of the Afghan block. The basin developed as a result of early Late (?) Cretaceous rifting between the once-connected Lut and Afghan cratonic blocks, but was relatively short-lived, eventually closing as the two blocks converged again in a NE–SW direction (in the present geographic orientation). This convergence was responsible for considerable folding and faulting in pre-Neogene times and also for emergence of the area during the Late Eocene to Oligocene. A dominantly Oligocene magmatic event is represented by widespread alkali volcanic rocks and minor intrusions that appear to be related to major

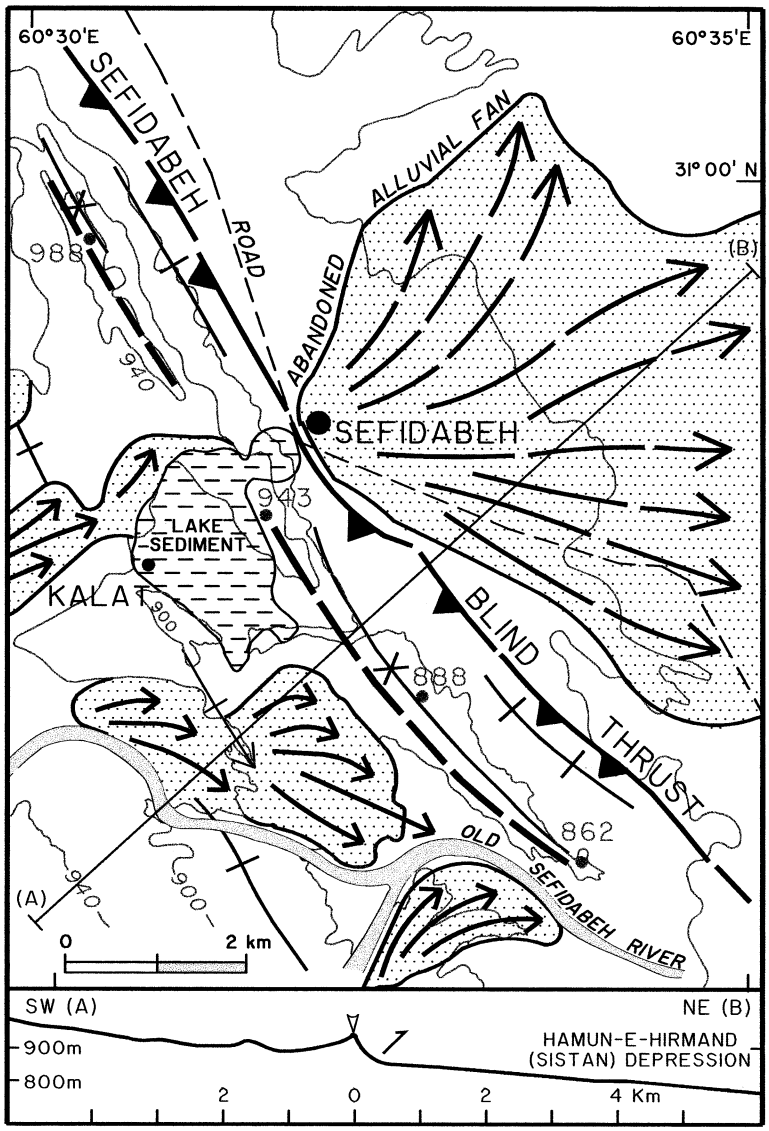

Figure 3. (Detailed map of the epicentral region of the 1994 Sefidabeh earthquakes. The discontinuous exposures of coseismic bedding-plane slip in 1994 occurred along the thick broken lines marked to the NW and SE of the abandoned Sefidabeh lake. The line of the Sefidabeh blind thrust is marked at the base of the hangingwall ridge (see Fig. 12b). The continuous thin lines are early Tertiary syncline (crosses) and anticline (ticks) axes. Abandoned older Quaternary alluvial fans (exact age unknown), with palaeoflow directions deduced from air photographs, are marked by stippled regions with broken arrows. Kalat-e-Haji is marked Kalat. The inset at the bottom is a SW–NE topographic profile through Sefidabeh along the line shown on the map, with the inverted triangle marking the location of 1994 bedding-plane slip.

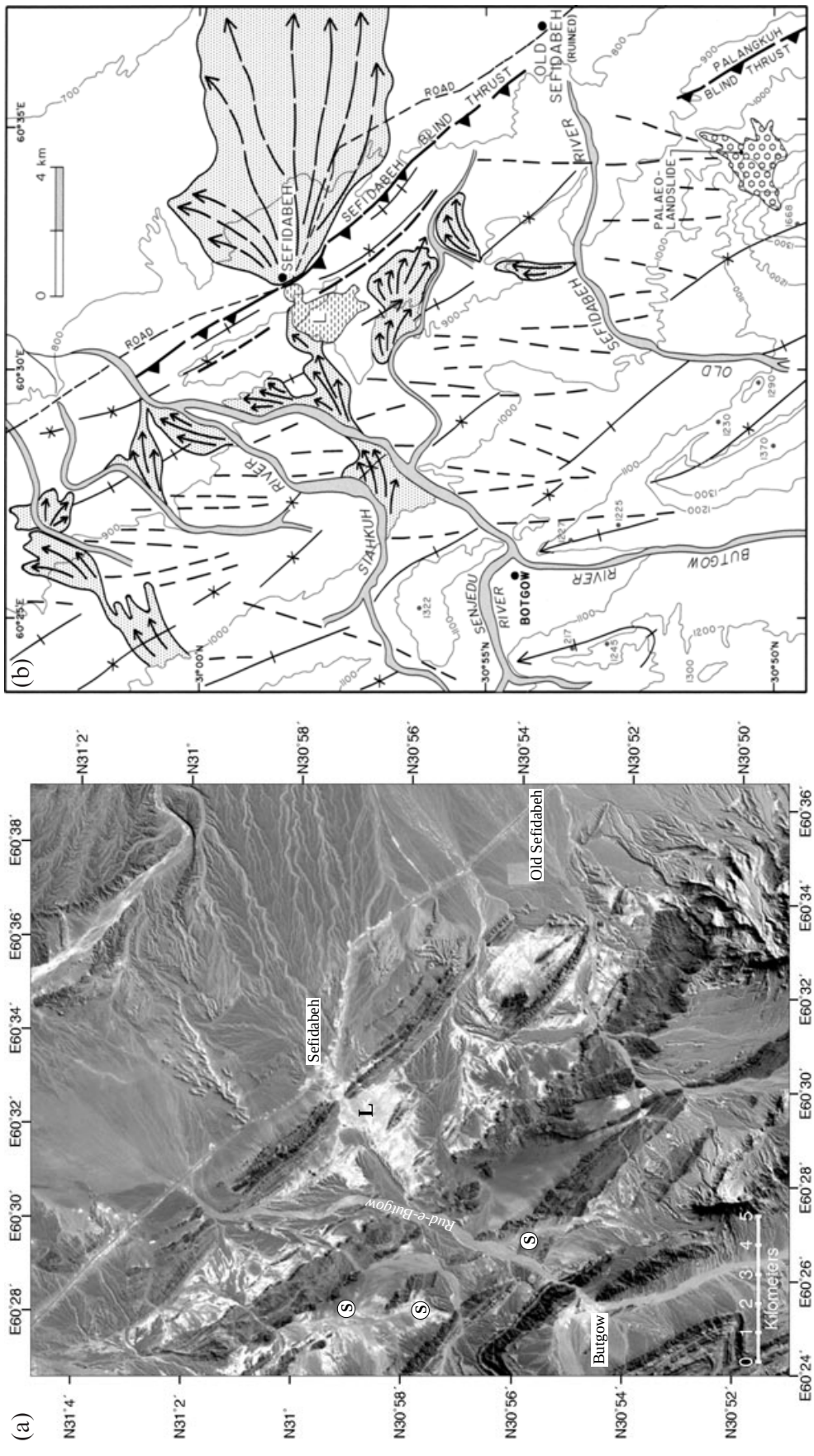

Figure 4. (a) LANDSAT TM image of the Sefidabeh region. The uplifted lake deposits near Sefidabeh are marked L and appear in white. Regions of minor N–S right-lateral strike-slip faulting, which offset volcaniclastic rocks, are marked S. The prominent line through Sefidabeh and Old Sefidabeh is the road from Neh to Zahedan. (b) Physiographic and structural map of the same region. Symbols as in Figs 3 and 13. The dashed N–S lines are minor strike-slip faults, some of them marked in Fig. 4(a), which are probably not active now (see text).

transcurrent faults. High-angle reverse faults with NW strikes are found in the cores of the tightest folds, which are commonly isoclinal in flysch. Early to mid-Tertiary deformation involved thrusts, folds and reverse faults with a (present-day) NW trend that are associated with, and sometimes cut by, a conjugate set of strike-slip faults, with N–S right-lateral faults dominant over smaller SE- to E-striking left-lateral faults (e.g. Freund 1970). Some of these same structures were probably reactivated in post-Miocene times as a result of the final Miocene–Pliocene collision between Arabia and Eurasia along the Zagros mountains in SW Iran (Freund 1970; Berberian 1981; Berberian & King 1981).

2.3 Active tectonics

Recent and active deformation in Sistan is dominated by N- to NNE-striking right-lateral strike-slip faults and NW-striking thrusts, related to the indentation of Iran by the Arabian shield (Figs 1 and 2). The Iran–Afghan border in Sistan is also a tectonic boundary, separating the distributed deformation in Iran from the virtually aseismic region of western Afghanistan, which is essentially part of the stable Eurasian plate. Convergence between Eurasia and Arabia is about 40 mm yr^{-1} at 60°E, some of which is taken up in the Zagros mountains in SW Iran, while the rest is accommodated mostly in the seismic belts of the Alborz and Kopeh Dagh in northern Iran, requiring the relatively aseismic region of central Iran to move N–NNE relative to Afghanistan (Fig. 1b). The N–S right-lateral shear component between central Iran and Afghanistan is taken up partly along the border in Sistan and partly on the western side of the Lut block. At the latitude of Sefidabeh the principal active structures are very large N- to NNE-striking right-lateral strike-slip faults such as the Zahedan, East and West Neh and Kahurak faults (Fig. 2a), with abundant evidence of displaced drainage systems and alluvial fans (e.g. Freund 1970; Camp & Griffis 1982; Tirrul *et al*. 1983). However, NW-striking thrusts indicate a significant shortening component across the belt as well. At its northern end, near 34°N, the Sistan belt ends in a system of E–W left-lateral faults that are thought to accommodate the N–S shear component by clockwise rotation (Jackson & McKenzie 1984; Jackson *et al*. 1995). To the south, near 27°N, the Sistan ranges merge with the E–W coastal ranges of the Makran, where the Arabian Sea is subducted northwards (e.g. Byrne *et al*. 1992).

3 THE 1994 SEFIDABEH SEQUENCE

3.1 Macroseismic effects

The 1994 sequence of earthquakes at Sefidabeh (*lit*. 'white water') started with a small foreshock on February 22, exactly 24 hr before the first large event of M_w 6.1 on February 23 at 08:02 GMT (11:30 local time). Four more events of M_w 5.5–6.2 followed over the next five days (Table 1). The first large event of February 23 caused six deaths (three in Sefidabeh and three in Kalat-e-Haji, 2 km SW of Sefidabeh) and injured 10 people, with damage to an estimated 300 buildings (200 were destroyed). The very low death toll for such an earthquake in Iran is related to the local time of the event and to the sparse population. Sefidabeh, on the Nehbandan–Zahedan road, is one of the few settlements of any size (population ~200) and was within 20 km of the instrumentally determined epicentre. Maximum intensities of about VII- (MMI) were observed at Sefidabeh and Kalat-e-Haji, but with such sparse data meaningful isoseismal maps cannot be drawn. The earthquakes fractured (VI) some buildings at Madeh Kariz (17 km NW of Sefidabeh), Karabasan (25 km to the NW), Umareh (29 km SSW) and Mok Sorkh (44 km SE). They were strongly felt (V) at Khunik (54 km NW), Neh (80 km NW), Zabol (92 km E) and Serahi (95 km SE).

3.2 Coseismic surface ruptures

On February 25, two days after the first damaging earthquake, discontinuous surface ruptures were observed in a zone 9.5 km long and 20 m wide trending NNW along the crest of the ridge SW of Sefidabeh village (Figs 3 and 4). It is not known in which of the first two events these ruptures formed. It is clear

Table 1. Source parameters of the main Sefidabeh earthquakes.

Date	Time	Lat.	Long.	Depth	m_b	M_s	M_w	M_0	Strike	Dip	Rake	TF	*sv*	R
1994.02.23	08:02:04	30.803	60.570	**7**	6.1	6.1	**6.05**	**1.51**	**143**	**29**	**96**	**2.7**	**46**	B
				15*			6.09	1.70	145	33	96	5.8	48	H
				22			5.99	1.20	123	27	91		32	U
1994.02.24	00:11:14	30.821	60.529	**10**	6.1	6.1	**6.20**	**2.54**	**155**	**45**	**110**	**6.1**	**38**	B
				15*			6.28	3.30	153	43	105	7.4	43	H
				20			6.12	1.90	168	40	121		40	U
1994.02.26	02:31:11	30.781	60.550	**5**	5.8	6.0	**5.95**	**1.06**	**146**	**36**	**107**	**3.6**	**35**	B
				15*			6.03	1.40	168	32	125	5.0	38	H
				22			5.91	0.91	156	33	113		39	U
1994.02.28	11:13:57	30.822	60.554	**6**	5.5	5.5	**5.49**	**0.22**	**122**	**33**	**78**	**1.9**	**36**	B
				15*			5.59	0.31	136	30	92	3.2	44	H
1994.02.23	11:54:33	30.768	60.551	15*	5.3	4.9	5.49	0.22	108	31	62	2.8	49	H

Epicentres are from Engdahl *et al.* (1998). Magnitudes (m_b and M_s) are from the USGS. Seismic moment (M_0) is in units of 10^{18} N m. TF is the duration of the time function in seconds, and *sv* is the slip vector azimuth, assuming that the SW-dipping nodal plane is the fault plane. The last column gives the origin of the earthquake source parameters on each line: from body wave modelling in this paper (B, shown in bold type), or from the CMT solutions by Harvard (H) or the USGS (U). The asterisk after the Harvard CMT depth indicates that it was fixed at 15 km in the inversion.

(a)

(b)

(c)

(d)

(e)

(f)

(g)

(h)

Figure 5. (*Continued.*)

from the seismological evidence (next section) that these surface ruptures were not on the fault or faults responsible for the earthquakes. The ruptures were all within the vertically dipping and isoclinally folded Upper Cretaceous–Palaeocene flysch and volcaniclastic rocks, and nearly all involved slip on bedding planes. The ruptures and scarps formed three types of surface feature.

(1) Discontinuous mini-grabens formed by double scarps and up to 1.7 m deep occurred along the Sefidabeh ridge crest (Figs 5a–d), with slip occurring on subvertical bedding planes, mostly in flysch. These grabens are well developed 1–2 km south of the gap in the ridge occupied by the old lake deposits adjacent to Sefidabeh (Fig. 4). Striations on the bedding planes showed subvertical dip slip, with no strike-slip component. The larger displacement was usually on the western wall of the mini-grabens. Exposures in gullies show that the 1994 movement increased previous offsets of at least 5.0 m on the same bedding planes, and that the saddle-like morphology of the ridge crest (Figs 5d and g) is the result of previous graben-forming movements.

(2) Step-like single scarps were also common on the Sefidabeh ridge, usually on the NE side and upthrown to the SW (Figs 5e and f), again on subvertical bedding planes.

(3) Other scarps on the ridge appeared to have formed by settlement of soft tuff beds between competent limestone layers (Fig. 5h), perhaps in response to the collapse of underground channels or caverns.

The dominant characteristic of the surface ruptures is bedding-plane slip, producing extensional features on the ridge. From the seismological and geomorphological evidence (see below), it appears that these ruptures formed in response to the growth of an anticline above a blind thrust. The mini-grabens in particular are reminiscent of those formed on the hangingwall anticline ridges at El Asnam in 1980 (Yielding *et al*. 1981) and Spitak in 1989 (Philip *et al*. 1992), although in those earthquakes bedding-plane slip was less important. Coseismic bedding-plane slip has been observed following other earthquakes in Iran, notably at Tabas in 1978 (Berberian 1979b). At Sefidabeh, the deformation responsible for the isoclinal folds with subvertical axes in the flysch pre-dates the formation of the ridge itself. It is difficult to relate the vertical bedding-plane slip seen in the 1994 coseismic ruptures to any particular style of thrust faulting deeper down: pervasive simple shear of the hangingwall may accommodate a change in fault dip at depth (see White *et al*. 1986, their Fig. 9), but does not require it. In any case, the early Tertiary deformation that caused tight isoclinal folding in the soft shale and flysch formations produced more discontinuous faulting within the harder limestones and tuffs (Freund 1970), and there is no certainty that the vertical bedding-plane shear seen at the surface extends to any great depth.

3.3 Seismology and earthquake source parameters

To provide better constraints on the source parameters of the main earthquakes in the sequence we analysed the body waveforms of the four largest events. We took digital broadband records from stations of the GDSN in the epicentral range 30–90° and convolved them with a filter that reproduces the bandwidth of the old WWSSN 15–100 long-period instruments. We then used the MT5 version (Zwick *et al*. 1995) of McCaffrey & Abers's (1988) and McCaffrey *et al*.'s (1991) algorithm, which inverts the *P* and *SH* waveform data to obtain the strike, dip, rake, centroid depth, seismic moment and source time function. We always constrained the source to be a double couple. The method and approach we used are described in detail elsewhere (e.g. Nabelek 1984; McCaffrey & Nabelek 1987; Molnar & Lyon-Caen 1989; Taymaz *et al*. 1991) and are too routine to justify repetition here.

The results of our inversions are shown in Figs 6–9 and Table 1. All four events that we analysed, and the additional Harvard CMT solution for an aftershock on February 23 (Table 1), have similar mechanisms involving reverse faulting with a NW strike and a nodal plane dipping SW at 29–45°. These five earthquakes all had epicentres (relocated by Engdahl *et al*. 1998) within 5 km of each other about 15 km south of Sefidabeh. The Sefidabeh ridge is the dominant active structure with a NW–SE orientation in the epicentral region, so that even allowing for a possible location error of 10–15 km, which is typical for instrumental epicentres in Iran after 1970 (Berberian 1979a), the epicentres and the location of

Figure 5. Field photographs of coseismic surface ruptures, all taken in February 1994. (a)–(c) Views looking SE on the Sefidabeh ridge crest 1 km south of Sefidabeh village. Coseismic ruptures all involved slip on subvertical bedding planes in Palaeocene flysch, forming mini-grabens. (d) Same region as (a)–(c), looking NW. Note the saddle-like morphology of the ridge crest, caused by previous bedding-plane slip and graben formation. (e) View NW along the Sefidabeh ridge crest, about 2 km S of Sefidabeh, which is visible in the background. Note the vertical bedding. (f) Same region as (e), looking SE. Single scarp in vertical flysch. (g) View SE along the Sefidabeh ridge crest from beyond the position of (f). Fractures in flysch and a saddle-like morphology. (h) Fissure formed within subvertical bed of soft tuff. Sefidabeh ridge, view SE.

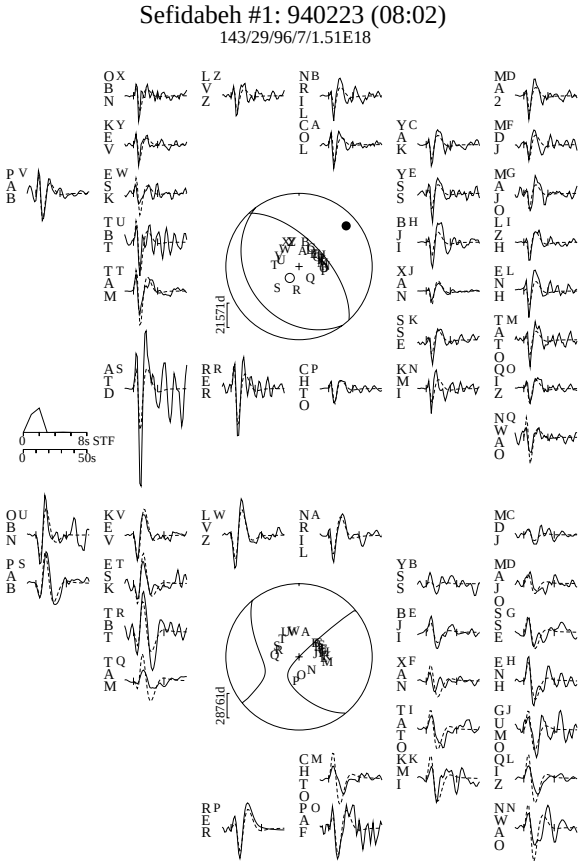

Figure 6. *P* (top) and *SH* (bottom) observed (solid) and synthetic (dashed) waveforms for the 23 February earthquake (Table 1). Station positions on focal spheres are identified by capital letters and arranged clockwise starting from north. STF is the source time function. Vertical ticks on the seismograms indicate the inversion window. Numbers beneath the header line are strike, dip, rake, centroid depth (km) and moment (N m). Stations were weighted according to azimuthal density and then *S* seismogram weights were halved, to compensate for their larger amplitudes. The *P* seismogram at ATD has an anomalous amplitude, probably because of an incorrectly reported magnification. This station was given half its normal weight in the inversions in Figs 6–9.

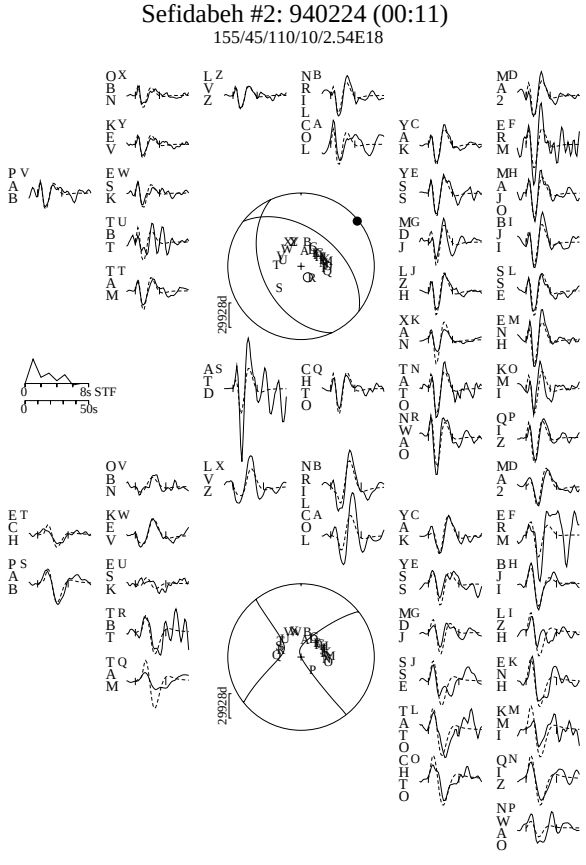

Figure 7. Observed and synthetic seismograms for the 24 February earthquake (Table 1). Layout and conventions are the same as in Fig. 6.

the coseismic ground fractures make faulting beneath the Sefidabeh ridge the likely cause of one or more of the 1994 earthquakes. Our main interest in these results is in how well the centroid depths and slip vectors are resolved, and because all the inversions share the same characteristics, these can be illustrated using the first event, on February 23.

Fig. 10 shows a selection of *P* and *SH* waveforms at different stations for the February 23 earthquake. In the first line is our final inversion result for this event, with a centroid depth of 7 km. The second and third lines show the results of inversions in which the depth was fixed at 12 and 3 km, but other parameters were free to change. The visual fit to the waveforms is worse in each case, with the width of the first cycle too broad at 12 km and too narrow at 3 km. By tests of this sort we estimate the centroid depth to be $7+4/-3$ km. These tests illustrate the nature of the trade-off between depth, time function duration and moment that is common for shallow dip-slip events. When forced to a shallow depth (line 3) the moment is greater and the time function longer. The opposite is true when forced to a greater depth (line 2). This is because of two effects. First, the time function compensates for the change in pulse width as the delay time between the direct ray and the surface reflections changes with depth. Second, the direct *P* wave and the surface reflections (*pP* and *sP*) generally interfere destructively at shallow depths because they have opposite polarities, requiring greater moment to achieve the observed amplitude on the seismogram. We carried out all the inversions in a half-space with $V_p = 6.5$ km s^{-1} and $V_s = 3.7$ km s^{-1}. Realistic changes in the velocity model make little change to the source orientation or depth, as shown in line 4 of Fig. 10, where the inversion used a 4-km-thick layer of $V_p = 6.0$ km s^{-1} above a half-space of $V_p = 6.8$ km s^{-1}. However, there is a significant change in the moment estimate associated with the different velocity structure and reflection coefficients. Thus we estimate the uncertainty in moment to be $\pm 0.2 \times 10^{18}$ or ~ 15 per cent.

The mechanisms for events 1, 3 and 4 (Figs 6, 8 and 9) of the sequence all share a steep NE-dipping nodal plane passing close to stations in the NE on the focal sphere. This leads to a significant trade-off between strike and rake on the SW-dipping plane (the one of interest to us under the Sefidabeh ridge), illustrated in Fig. 11. Fig. 11 follows the format of Fig. 10, but with the strike of the SW-dipping plane fixed at values up to $\pm 40^\circ$ different from the final result (middle line), while all other parameters are allowed to change in the inversion. It can be seen that the rake changes systematically with the strike, so as to maintain the steep NE-dipping nodal plane in its same position on the focal sphere. In all five inversions in Fig. 11 the

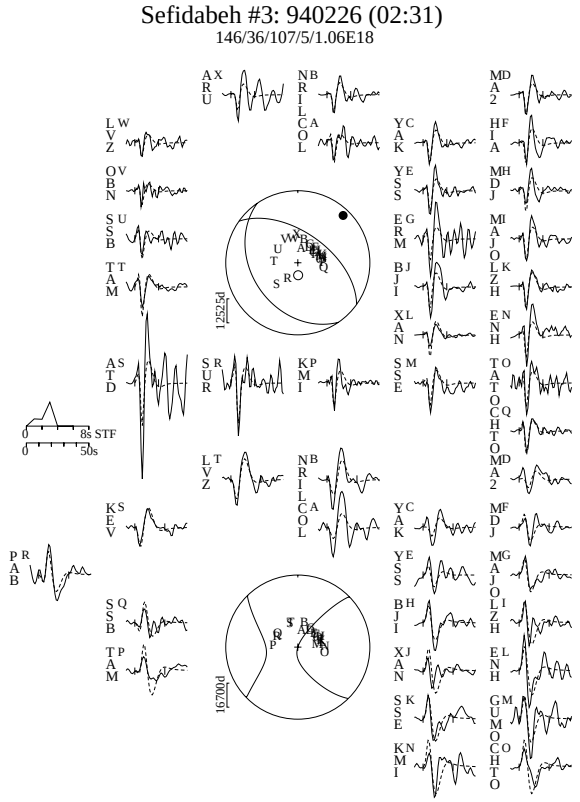

Figure 8. Observed and synthetic seismograms for the 26 February earthquake (Table 1). Layout and conventions are the same as in Fig. 6.

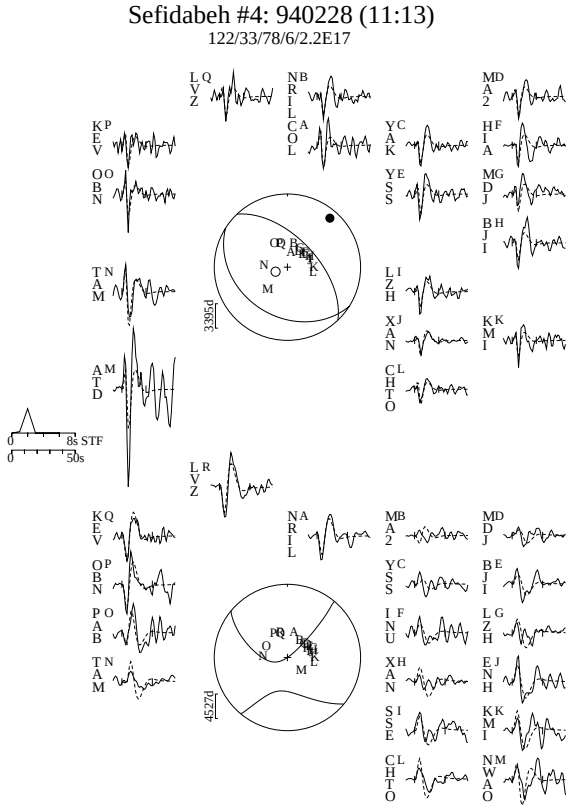

Figure 9. Observed and synthetic seismograms for the 28 February earthquake (Table 1). Layout and conventions are the same as in Fig. 6.

strike of the NE-dipping plane, and hence the slip vector azimuth if the SW-dipping plane is the fault plane, varies by less than $\pm 10^\circ$. Thus although we estimate the uncertainty in strike ($\pm 40^\circ$) and rake ($\pm 30^\circ$) to be quite large, the slip vector is well resolved to be in direction $047 \pm 10^\circ$, which is important for our later discussion. In fact, the strike of the Sefidabeh ridge is 145°, which is very close to the 143° obtained in our final inversion. Similar tests show that the dip of the SW-dipping plane is tightly constrained to $\pm 5^\circ$, controlled by the immobility of the NE-dipping plane in the inversion.

All the events of the sequence have similar focal mechanism orientations (Table 1), in particular with the dips of the SW-dipping planes in the range 29°–45°, slip vector azimuths (assuming the fault plane dips SW) in the range 36°–46°, and centroid depths in the range 5–10 km. There is no correlation of dip with depth that we can resolve, and no indication from these earthquakes that the reverse faults at shallow depths flatten onto horizontal surfaces within the seismogenic upper crust. The source parameters we obtained from body wave inversion are similar to those obtained by the Harvard and USGS CMT inversions (Table 1), which are within our estimated uncertainties except for centroid depth and moment. We expect our depths to be better resolved because we used higher frequencies, and differences in moment are probably related to different velocity structures and depths (see Fig. 10).

3.4 Geomorphology and fault growth

The Sefidabeh ridge contains several Late Quaternary geomorphological features associated with its tectonic activity and uplift. Across-ridge profiles are asymmetric, with an abrupt, steep NE side, and typically have an eroded saddle-like morphology observed where mini-graben form due to slip on bedding surfaces. In addition, rivers crossing the ridge incise gorges, leaving abandoned fans and terraces on the uplifted SW side (e.g. near 30°52′N 60°35′E in Fig. 4a). Large ancient landslides, which may have been triggered by earthquakes, are present along the steep ridge flank at 30°50′N 60°34′E, 15 km SE of Sefidabeh (Fig. 4b). However, by far the most dramatic feature is an abandoned playa with lake bed deposits (marked L in Figs 4a and b) 1 km SW of Sefidabeh village itself (Fig. 12). These deposits were formed by an ancient stream that once crossed the ridge and was blocked, presumably in part by uplift of the ridge. The light-coloured lake sediments are restricted to the ridge and are now ~70 m above the Sefidabeh plain and also above the level of the present Butgow river, which currently flows around the NW end of the ridge (Figs 4a and b). Palaeodrainage through the gap in the ridge now occupied by the lake deposits was responsible for the formation of abandoned fans and stream channels NE of Sefidabeh, which have lost their catchment. The lake deposits contain travertine that can potentially be dated. We observed no obvious folding of the lake sediments as a result of anticline growth, but this is not surprising: the wavelength of surface folding depends on the down-dip length of the underlying blind reverse fault and is therefore likely to be ~10–15 km (e.g. Savage & Hastie 1966), which is far broader than the narrow exposure on the Sefidabeh ridge itself. Other stream diversions with abandoned fans and stream channels are present along the Siahkuh river north of Butgow and the Old Sefidabeh river south of modern Sefidabeh

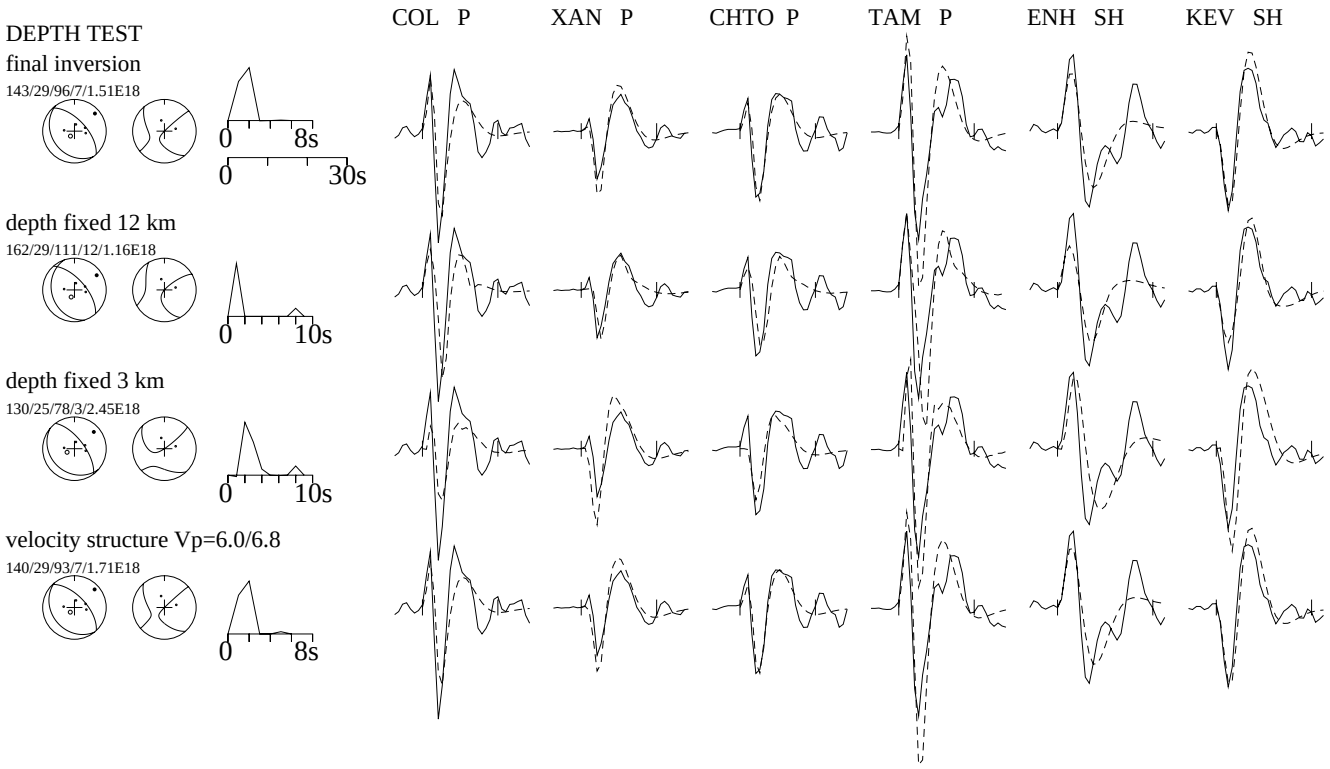

Figure 10. Tests to check the inversion for the 23 February event (Fig. 6) for the sensitivity to centroid depth. Synthetic seismograms are dashed, observed are solid lines. The first line contains seismograms from Fig. 6 and the final inversion result. *P* and *SH* focal spheres are shown, with the time function and numbers showing the strike, dip, rake, depth and moment. In the second and third lines the depth has been fixed at 12 and 3 km. In the fourth line a different velocity structure was used, with a layer 4 km thick of $V_p = 6.0$ km s^{-1} above a half-space of $V_p = 6.8$ km s^{-1}. In all other inversions a half-space of $V_p = 6.5$ km s^{-1} was used. See text for discussion.

(Fig. 4b). A tentative evolution of the palaeochannels and alluvial fans with respect to the Sefidabeh ridge uplift is illustrated in Fig. 13.

The diversion of the Butgow and Siahkuh rivers to the NW, around the end of the growing hangingwall anticline ridge, closely resembles the drainage patterns described on other active hangingwall anticlines in Otago, New Zealand (Jackson *et al*. 1996), the western Transverse Ranges of California (Keller *et al*. 1998, 1999) and the Tell Atlas of Algeria (Boudiaf *et al*. 1998), all of which have been attributed to lateral growth or propagation of the underlying fault with time.

Without geodetic data to determine coseismic elevation changes at Sefidabeh, we can only estimate crudely the likely changes resulting from these earthquakes. Let us consider the first main event of the sequence and assume arbitrarily a down-dip rupture width (W) of 10 km, corresponding to slip on a plane dipping 30° between depths of 4.5 and 9.5 km (either side of the centroid at 7 km). If we also assume a ratio of average slip to length of 5×10^{-5}, which is typical of intraplate earthquakes (e.g. Scholz *et al*. 1986) and a rigidity of 3×10^{10} N m^{-2}, then from the seismic moment of 1.5×10^{18}N m we would estimate a fault length (L) of 10 km and an average slip of 0.5 m. Since $L \propto W^{1/2}$ in our calculation, a change in our assumed value of W does not greatly affect these estimates. In this case our assumption of $W = 10$ km gives a fault with a roughly 1:1 aspect ratio of dimension 10 km, compatible with the time function duration of ~3 s in the body wave inversion (Table 1), assuming a typical rupture velocity of ~3.5 km s^{-1}. The morphology of the Sefidabeh ridge suggests the underlying fault segment is ~15 km long, with Sefidabeh roughly at its centre, ending near Old Sefidabeh in the SE (Fig. 4), where another segment in a right-stepping *en echelon* position (the Palangkuh Thrust, Fig. 4b) continues this orientation of thrusting further SE to the Zahedan Fault (Figs 2 and 14a).

Thus it is probable that slip on the fault underlying the Sefidabeh ridge occurs in increments of the order of 0.5–1.0 m, producing uplift of the order of 0.25–0.5 m in each event, and requiring 150–300 earthquakes to uplift the lake deposits by 70 m. If, during this time, the ridge has propagated from Sefidabeh to its present terminus 7 km to the NW, then the propagation rate per earthquake is of the order of 25–50 m. Perhaps coincidentally, these values for incremental growth are close to those estimated for fault segments of similar length in Nevada (30–50 m; Jackson & Leeder 1994) and New Zealand (10–50 m; Jackson *et al*. 1996) using similar geomorphological arguments. More sophisticated estimates can also be made, which allow for the incremental growth in fault length as well as for the observed scaling of coseismic displacement with length. In Cowie & Scholz's (1992a) theoretical model of fault growth, the number of earthquakes (N) required to increase the length of a fault from an initial value L_0 to a length L is

$$N = \frac{\log L/L_o}{\log (1 + \alpha/\gamma)}, \tag{1}$$

where α is the ratio of the mean slip during an earthquake to the rupture length, and γ is the ratio of the mean accumulated displacement on a fault to its length. The ratio $r = \alpha/\gamma$ is the proportional increase in fault length during each earthquake.

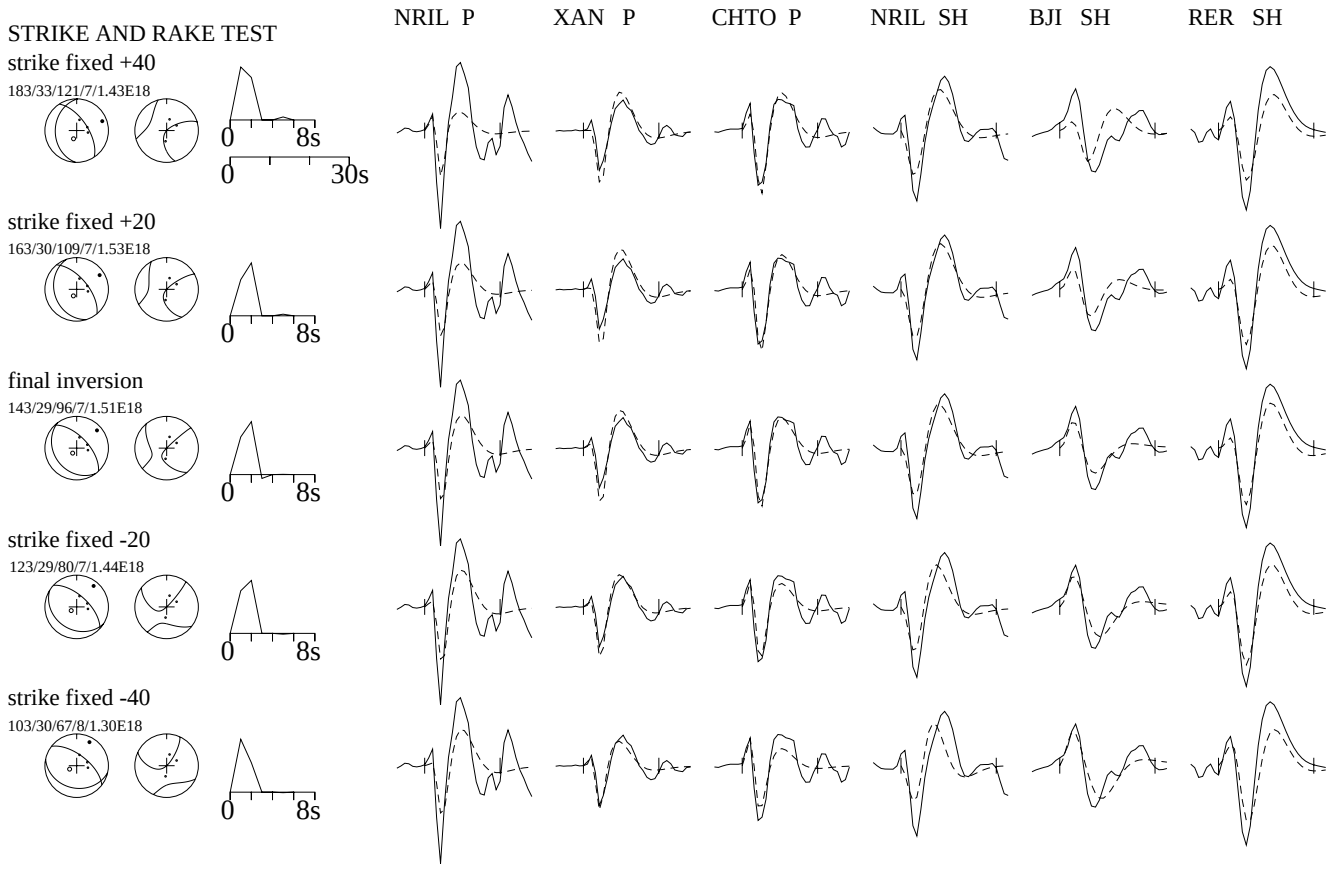

Figure 11. Tests to illustrate the trade-off between strike and rake and the consistent orientation of the NE-dipping nodal plane in the inversion for the 23 February earthquake (Fig. 6). See text for discussion.

The expected value of α is about 5×10^{-5} for continental earthquakes (Scholz *et al*. 1986), and the expected value of γ for faults of length $\sim$10–20 km is $\sim10^{-2}$ (Cowie & Scholz 1992b) The ratio r is then $\sim1.5\times10^{-3}$ or 0.15 per cent. Thus in this model the Sefidabeh Fault segment, currently $\sim$15 km long, would be expected to grow by 23 m per earthquake, a number that is not significantly different from the more simplistic estimate based on geomorphology. If we consider the propagation of the last 7 km at the NW end of the Sefidabeh ridge, then $L/L_0\sim1.9$, and the expected number of earthquakes required to achieve this growth is 420 (from eq. 1).

These very crude calculations suggest, first, that lateral growth per earthquake is too small to recognize after any single event, and second, that the lake beds have been uplifted by hundreds of earthquakes and may be of the order of 0.1–1.0 Myr old if recurrence times are of the order of 1000 yr.

3.5 Other earthquakes in the area

Given the remote nature of this region, its historical earthquake record is almost certainly incomplete. Large earthquakes with surface rupture are known further north in the Sistan suture zone at Nauzad in 1493, on another NW-striking thrust (Fig. 14b, and Ambraseys & Melville 1982), and in the present century along the N–S right-lateral Abiz Fault, including the M_w 7.2 Zirkuh earthquake of 1997 (Berberian *et al*. 1999). In this southern area, a large earthquake near Nosratabad (Fig. 2b) in 1838 is thought to have produced N–S ground ruptures, presumably on the right-lateral Nosratabad Fault (Ambraseys & Melville 1982; Berberian & Yeats 1999).

Other evidence for past earthquakes is conjectural. The ancient settlement of Shahr-e-Sukhthe (*lit*. 'the burnt city') SW of Zabol, which flourished around 2000 BC, was abandoned when the Hirmand river altered its course by 90° for reasons that are unknown, and may not be tectonic in origin (Matheson 1976).

In modern instrumental times the Sefidabeh region has been relatively quiet. Two other Harvard CMT solutions (Fig. 2b) show N–S right-lateral strike-slip faulting near Neh on 1990.03.15 (M_w 5.1) and thrusting on a similar trend to the 1994 earthquakes on 1992.09.11 east of Nosratabad (M_w 5.3).

4 RELATIONS BETWEEN STRIKE-SLIP FAULTING AND THRUSTING IN EASTERN IRAN

The southern Sistan ranges in the Sefidabeh region accommodate a combination of N–S right-lateral shear and shortening between the Dasht-e-Lut and Afghanistan (e.g. Fig 1b). South of 34°N, this motion is achieved by N- to NNE-striking right-lateral strike-slip faults and NW–SE-striking thrust or reverse faults such as that at Sefidabeh. These faults are clear

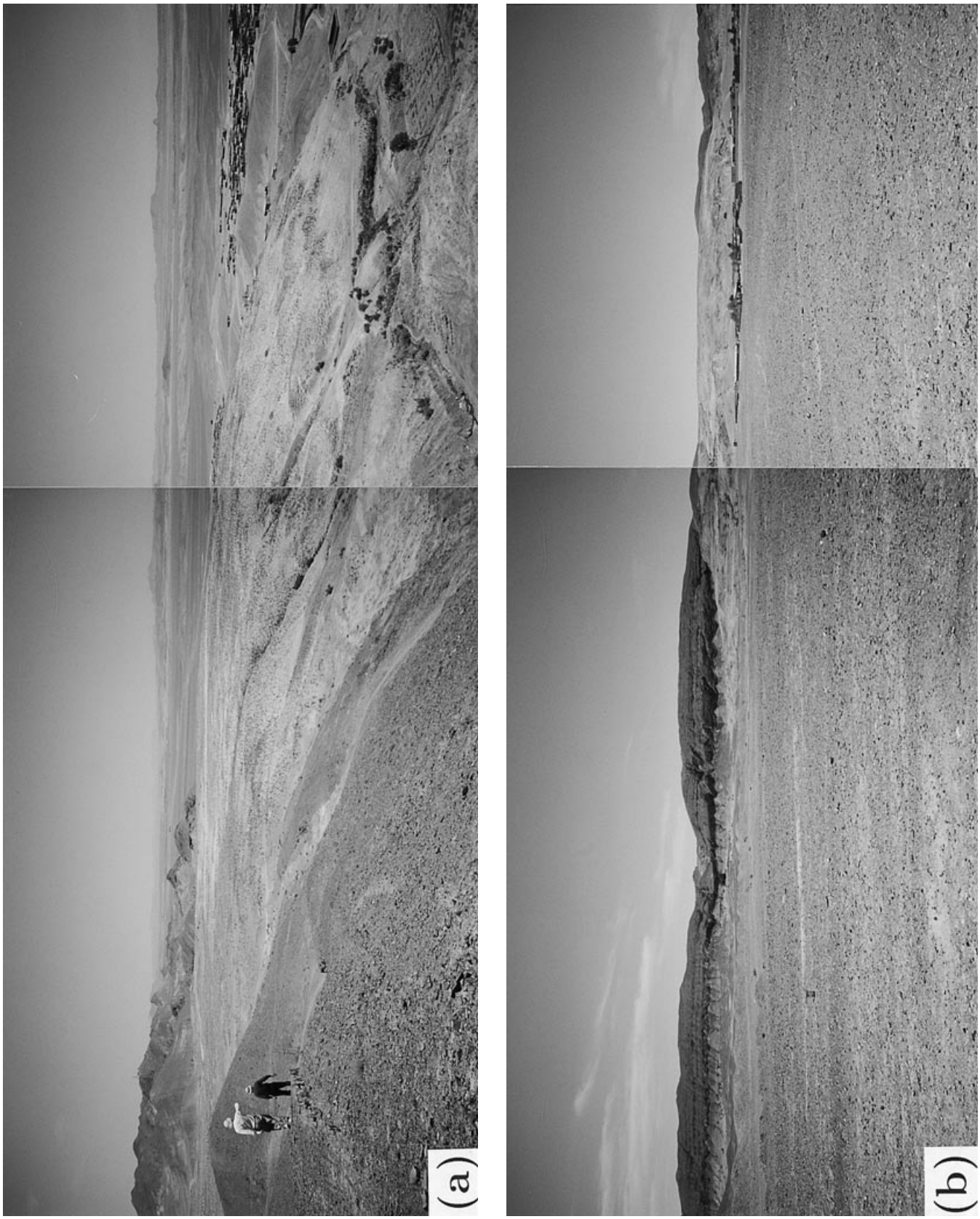

Figure 12. Two views of the uplifted lake deposits on the Sefidabeh ridge. (a) View N across the lake playa from the Sefidabeh ridge. In the distance on the left is the northern part of the ridge, with the telecommunication tower. On the right is Sefidabeh village. The lake deposits form a flat light-coloured surface occupying the gap in the ridge, now about 70 m above the Sefidabeh plain. The people in the foreground are a few hundred metres north of the location of Figs 5(a)–(d). (b) View SW to the Sefidabeh ridge from the main road at Sefidabeh (see Fig. 4). On the right is Sefidabeh village, and behind it are the light-coloured uplifted lake beds forming a low dip in the ridge skyline.

in the satellite imagery, air photographs, geomorphology and geology (e.g. Freund 1970; Camp & Griffis 1982; Tirrul *et al*. 1983; Berberian *et al*. 1999; Berberian & Yeats 1999) and earthquake focal mechanisms show only these two types, with slip vectors directed N–S on the strike-slip faults and NE–SW on the reverse faults (Fig. 2a). Although the two fault (and earthquake) types share the same NE–SW axis of principal shortening, the kinematics of this fault system are not straightforward and are the subject of this section.

Freund (1970) realized that the association of strike-slip and thrust faults in Sistan was likely to involve rotations about a vertical axis. In his scheme, the right-lateral strike-slip faults rotate anticlockwise away from the roughly NE–SW direction of maximum shortening. We believe that his scheme is correct in principle, and we can now examine more closely the relation between the strike-slip and thrust faults. An important feature of the roughly N–S strike-slip faults in Sistan is that they are not continuous along the whole length of the zone from 28 to 34°N, even though individual faults commonly exceed 100 km in length. Many of the thrusts in Sistan splay from these strike-slip faults and die away with distance from them, with some of the most prominent thrusts occurring at the ends of the strike-slip faults, which can be very abrupt. The Sefidabeh Thrust is a good example, splaying NW from the northern terminus of the right-lateral Zahedan Fault, and dying away to the NW (Fig. 14a). The highest topography is associated with the junction of the strike-slip and thrust faults at Palang Kuh (+2029 m), with the ridge falling to ~900 m near Sefidabeh itself. A similar geometry is seen further north at 33°N (Fig. 14b), where the Nauzad Fault (responsible for the 1493 earthquake) splays NW off the north end of the Purang Fault system (Berberian *et al*. 1999). Thrust faults splaying off the east side of the strike-slip faults strike SE and also die out in that direction. Examples include the Bandan Fault (Fig. 2b), splaying off the East Neh Fault, and the southern terminus of the Abiz Fault near 33°N, where the 125-km-long N–S strike-slip rupture in the 1997 Zirkuh earthquake terminated in a SE-striking thrust (Berberian *et al*. 1999).

When viewed as a whole, the Sistan region of eastern Iran is simply a N–S belt about 100 km wide that accommodates NE–SW shortening. It could accommodate this motion by a system involving only NW–SE thrust or reverse faults with NE slip vectors, and there are indeed plenty of thrusts with this orientation and slip vector. Yet the striking feature of the fault system in Sistan is the presence of long N- to NNE-striking right-lateral strike-slip faults terminating in relatively short thrusts that splay off their ends and die away with distance from them. The role of major intracontinental strike-slip faults in convergent settings is usually either (a) lateral expulsion of material along strike, (b) partitioning of oblique convergence into strike-slip and thrust components, or (c) rotation about a

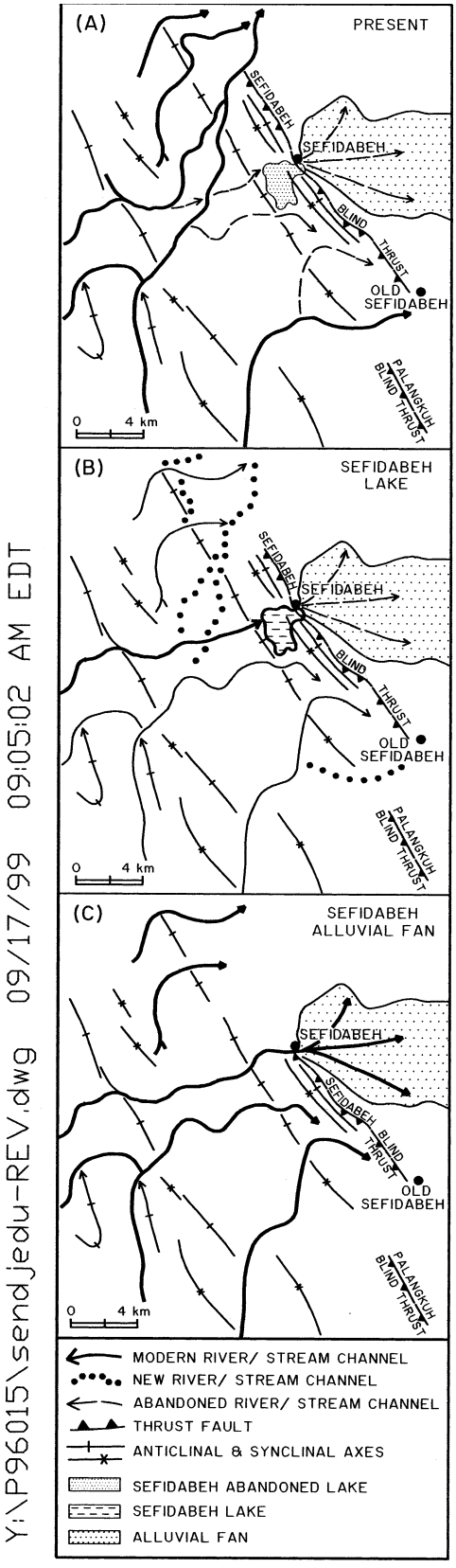

Figure 13. A tentative evolution of the stream system near Sefidabeh in response to the growing hangingwall anticline above the Sefidabeh blind thrust and the northward propagation of the thrust tip. (a) The present-day configuration, showing the abandoned lake bed near Sefidabeh. (b) The situation just prior to the abandonment of the lake, with future (i.e. present-day) stream channels dotted. (c) An older Quaternary configuration (exact age unknown), when the hangingwall ridge was lower and the alluvial fan at Sefidabeh was still active. This figure is to illustrate the nature of the changes that occurred to the drainage system, rather than the timing. It is tentative because we do not know that changes to the Old Sefidabeh, Butgow and Siahkuh rivers (identified in Fig. 4b) happened simultaneously; indeed, it is perhaps unlikely that they did so.

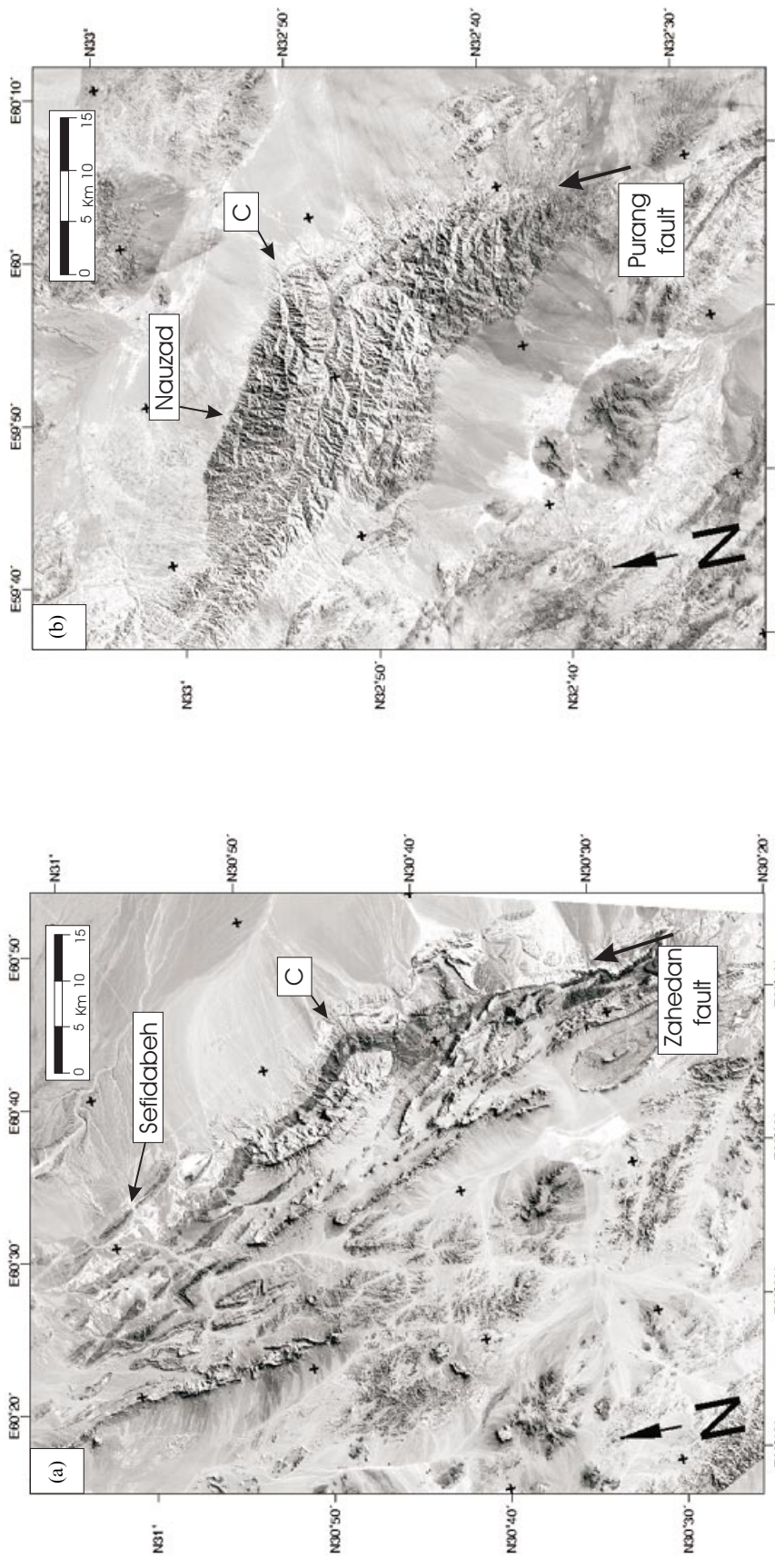

Figure 14. Two LANDSAT TM images showing the abrupt termination of major N–S right-lateral strike-slip faults in the southern Sistan suture zone at their junctions (marked C) with thrusts splaying off to the NW. (a) The northern end of the Zahedan Fault and its junction with the SE end of the Sefidabeh Thrust system (see also Figs 2b and 4a). (b) The northern end of the Purang strike-slip system and its junction with the Nauzad Thrust, near 33°N (see Berberian *et al.* 1999).

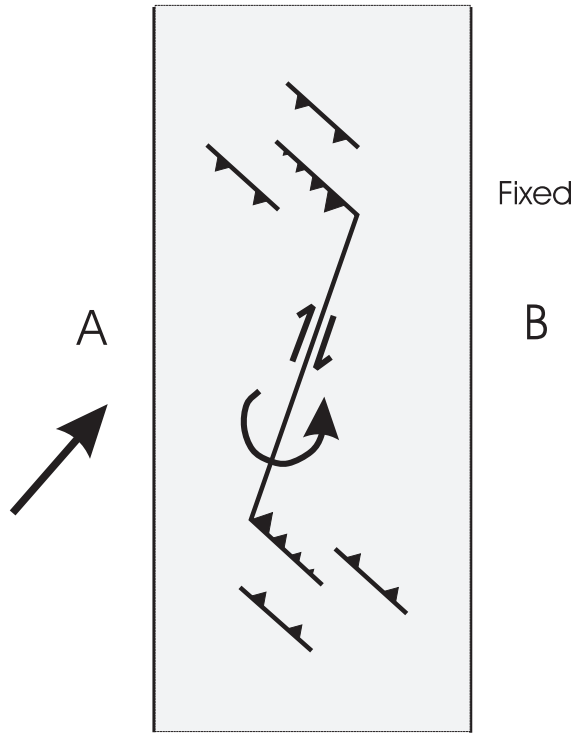

Figure 15. Cartoon to illustrate the accommodation of overall NE–SW shortening (large arrow) across a deforming zone (shaded) between two rigid blocks or plates (A and B) by a rotating strike-slip fault. The strike-slip fault terminates in thrust faults whose displacements die away with distance from their intersections with the strike-slip fault, thus allowing the anticlockwise rotating strike-slip fault to be spatially associated with other thrusts that do not need to rotate. A similar geometry is seen in Mongolia (Bayasgalan *et al.* 1999). Note that the blocks bounding the strike-slip fault cannot be rigid, but must also deform.

vertical axis. In Sistan, the long right-lateral strike-slip faults cut across the general trend of the belt (Fig. 2a) with NNE–SSW slip vectors that are not parallel to the NE–SW slip vectors on the thrusts. In addition, there are no major E–W left-lateral conjugate strike-slip faults south of 34°N (Fig. 2). These geometric features suggest that south of 34°N the overall NE–SW convergence is achieved by the N–S right-lateral strike-slip faults rotating anticlockwise relative to the Lut and Afghan blocks (Fig. 2), and that thrusts such as those at Sefidabeh and Nauzad accommodate this rotational deformation at their ends. This geometry is illustrated in Fig. 15 and is similar to that described in Mongolia by Bayasgalan *et al.* (1999). The key feature of this pattern is that the thrusts splaying from the strike-slip faults allow the rotating strike-slip faults to be spatially mixed with other NW–SE thrusts that do not need to rotate. Thus we concur with Freund (1970) that anticlockwise rotations about a vertical axis are an essential feature of the deformation in Sistan.

However, the cartoon in Fig. 15 is a simplification of what must occur. Since the slip vectors on the thrusts and strike-slip faults are different, the blocks bounding the strike-slip faults cannot be rigid and must deform internally. Thus, although the decrease in displacement on the thrusts with distance from the strike-slip fault terminations implies rigid rotations about poles near the ends of the thrusts, this interpretation is almost certainly too simplistic (see Bayasgalan *et al.* 1999). Moreover, the strike-slip faults do not mark the edges of the deforming zone, which would prevent them from rotating, nor do they bound rigid blocks. Certainly, a great deal of deformation is seen away from the major strike-slip and thrust faults (Fig. 2 and Freund 1970), but it is not easy to distinguish structures that are active now from earlier Tertiary deformation. For example, the region SW of Sefidabeh contains numerous N–S minor right-lateral strike-slip faults (Fig 4a and b), visible mostly in more competent limestone and volcaniclastic rocks. These minor faults mostly terminate in isoclinal folds within the flysch and probably pre-date the formation of the Sefidabeh ridge. There is no indication that they cut Late Quaternary fan or outwash surfaces. The need for internal deformation is reduced if the strike-slip faults have a reverse component, but there is little indication of this in the earthquake mechanisms (see also Berberian *et al.* 1999). On the other hand, the N–S strike-slip faults are associated with N–S mountain ranges, which suggests that shortening does occur, though not necessarily on the strike-slip faults themselves.

The kinematic arrangement in Sistan is different from those seen in many other continental regions of oblique shortening. 'Partitioning' or separation of the oblique motion into its strike-slip and convergent components on subparallel faults with orthogonal slip vectors is seen in a number of places such as central California (Mount & Suppe 1987), Papua New Guinea (Abers & McCaffrey 1988) and western Pakistan (Lawrence *et al.* 1992). All of these places are characterized by major throughgoing strike-slip faults, unlike the faults that abruptly end in Sistan, and do not require rotations about a vertical axis. Rotations are known in the western Transverse Ranges of California (e.g. Luyendyk *et al.* 1980), but in a clockwise sense within a right-lateral shear setting on a system of thrusts that are not connected to strike-slip faults in the same way as they are in Sistan (e.g. Molnar & Gipson 1994).

Bayasgalan *et al.* (1999) described similar fault configurations in Mongolia to those seen in Sistan. They make the point that the strike-slip terminations that end in thrusts may be temporary if the strike-slip faults grow past the thrusts to link up with other fault segments beyond (see also Meyer *et al.* 1998). This process will lead to the formation of longer, more continuous, throughgoing strike-slip faults, which will eventually rotate to become parallel to the boundaries of the deforming belt. At that point a separation of the strike-slip and convergent components of motion across the zone could occur, with the thrusts perhaps rotating (clockwise in Sistan) into a configuration parallel to the strike-slip faults and also becoming longer. Seen in this light, the Sistan belt of eastern Iran may be in an early stage of development on the way to the 'partitioned' configuration seen in western Pakistan, where the N–S right-lateral Chaman Fault is adjacent to the long N–S thrusts of the Kirthar ranges (e.g. Lawrence *et al.* 1992). A similar development involving the rotation of thrust faults seems to have occurred adjacent to the San Andreas Fault in central California (Miller 1998).

Thus the style of faulting in oblique convergent zones such as Sistan may depend on the availability of throughgoing strike-slip faults, which, in turn, may depend on the total amount of strike-slip motion across the zone. Arabia has moved about 200 km north into Iran since the closure of the Zagros suture in the Pliocene, but only a fraction of that has to be accommodated in Sistan, because some is taken up by shortening in

the Zagros and by other N–S strike-slip faults west of the Dasht-e-Lut. Faulting in Sistan may still be dominated by reactivation of relatively discontinuous structures inherited from the Eocene closure of the suture zone.

5 CONCLUSIONS

The 1994 Sefidabeh earthquake sequence was significant for two reasons. First, it provided a fine example of the geomorphological features at the surface associated with blind thrusting at depth, including insights into how such features evolve with time. Examples of this sort increase our ability to recognize active structures that are important for seismic hazard and active tectonic evaluations. Second, it drew attention to the close association between the thrust and strike-slip faulting in Sistan, and how major intracontinental strike-slip faults can apparently terminate abruptly within deforming regions. The fault configurations that are seen in Sistan almost certainly require rotations about a vertical axis, but may be a stage on the way to a more evolved state involving partitioning of strike-slip and thrust components onto separate subparallel faults.

ACKNOWLEDGMENTS

MB and JAJ thank M. T. Khorehei and M. Qorashi of the Geological Survey of Iran for logistical support in Iran, for MB's airfares, and for their sustained enthusiasm for our joint studies over several years. We are grateful to M. Oliyazadeh of the University of Industries and Mines (Ministry of Mines and Metals) for accommodation in Birjand, Birjand University for transportation in the Sefidabeh area, and A. A. Karimabadi for long hours of driving in demanding conditions. We thank Christine Johnson for drafting, M. Goldsworthy and A. Bayasgalan for help with satellite imagery, E. Keller, A. Sylvester and A. Nicol for constructive reviews and the Royal Society for a travel grant. Maps were produced with the GMT software of Wessel & Smith (1995). Cambridge Earth Sciences contribution ES 5876. This paper is dedicated to the memory of N. Khadem, founder and managing director of the Geological Survey of Iran from 1962 to 1974, who died on 4 May 1999, while the fieldwork for this paper was being completed.

REFERENCES

Abers, G. & McCaffrey, R., 1988. Active deformation in the New Guinea fold-and-thrust belt: seismological evidence for strike-slip faulting and basement-involved thrusting, *J. geophys. Res.,* **93,** 13 332–13 354.

Ambraseys, N.N. & Melville, C.P., 1982. *A History of Persian Earthquakes,* Cambridge University Press, New York.

Bayasgalan, A., Jackson, J., Ritz, J.-F. & Cartier, S., 1999. Field examples of strike-slip fault terminations in Mongolia and their tectonic significance, *Tectonics,* **18,** 394–411.

Berberian, M., 1979a. Evaluation of instrumental and relocated epicentres of Iranian earthquakes, *Geophys. J. R. astr. Soc.,* **58,** 625–630.

Berberian, M., 1979b. Earthquake faulting and bedding thrust associated with the Tabas-e-Golshan (Iran) earthquake of September 16, 1978, *Bull. seism. Soc. Am.,* **69,** 1861–1887.

Berberian, M., 1981. Active faulting and tectonics of Iran, in *Zagros–Hindu Kush–Himalaya Geodynamic Evolution,* eds Gupta, H.K. & Delany, F.M., *Am. geophys. Un., Geodyn. Ser.,* **3,** 33–69.

Berberian, M. & King, G.C.P., 1981. Towards a paleogeography and tectonic evolution of Iran, *Can. J. Earth Sci.,* **18,** 210–265.

Berberian, M. & Yeats, R.S., 1999. Patterns of historical earthquakes rupture in the Iranian plateau, *Bull. seism. Soc. Am.,* **89,** 120–139.

Berberian, M., Jackson, J.A., Qorashi, M., Khatib, M.M., Priestley, K., Talebian, M. & Ghafuri-Ashtiani, M., 1999. The 1997 May 10 Zirkuh (Qa'enat) earthquake (M_w 7.2): faulting along the Sistan suture zone of eastern Iran, *Geophys. J. Int.,* **136,** 671–694.

Boudiaf, A., Ritz, J-F. & Philip, H., 1998. Drainage diversions as evidence of propagating active faults: example of the El Asnam and Thenia faults, Algeria, *Terra Nova,* **10,** 236–244.

Building and Housing Research Center, 1994. *Preliminary Report on the Sefidabeh (Sistan va Baluchistan) Earthquake of Esfand 4, 1372,* Rept 5, Building and Housing Research Center, Tehran (in Persian).

Bullard, T.F. & Lettis, W.R., 1993. Quaternary fold deformation associated with blind thrust faulting, Los Angeles basin, California, *J. geophys. Res.,* **98,** 8349–8369.

Byrne, D.E., Sykes, L.R. & Davis, D.M., 1992. Great thrust earthquakes and aseismic slip along the plate boundary of Makran subduction zone, *J. geophys. Res.,* **97,** 449–478.

Camp, V.E. & Griffis, R.J., 1982. Character, genesis and tectonic setting of igneous rocks in the Sistan suture zone, eastern Iran, *Lithos,* **3,** 221–239.

Cowie, P.A. & Scholz, C.H., 1992a. Growth of faults by accumulation of seismic slip, *J. geophys. Res.,* **97,** 11 085–11 095.

Cowie, P.A. & Scholz, C.H., 1992b. Displacement-length scaling relationship for faults: data synthesis and discussion. *J. struct. Geol.,* **14,** 1149–1156.

Engdahl, E.R., van der Hilst, R. & Buland, R., 1998. Global teleseismic earthquake relocation with improved travel times and procedures for depth determination, *Bull. seism. Soc. Am.,* **88,** 722–743.

Freund, R., 1970. Rotation of strike-slip faults in Sistan, southeast Iran, *J. Geol.,* **78,** 188–200.

Jackson, J.A. & Leeder, M.R., 1994. Drainage systems and the development of normal faults: an example from Pleasant Valley, Nevada, *J. struct. Geol.,* **16,** 1041–1059.

Jackson, J.A. & McKenzie, D.P., 1984. Active tectonics of the Alpine-Himalayan belt between western Turkey and Pakistan, *Geophys. J. R. astr. Soc.,* **77,** 185–264.

Jackson, J.A., Haines, A.J. & Holt, W.E., 1995. The accommodation of Arabia–Eurasia plate convergence in Iran, *J. geophys. Res.,* **100,** 15 205–15 219.

Jackson, J.A., Norris, R. & Youngson, J., 1996. The structural development of active fault and fold systems in central Otago, New Zealand: evidence revealed by drainage patterns, *J. struct. Geol.,* **18,** 217–234.

Keller, E.A., Zepeda, R.L., Rockwell, T.K., Ku, T.L. & Dinklage, W.S., 1998. Active tectonics at Wheeler Ridge, southern San Joaquin Valley, California. *Geol. Soc. Am. Bull.,* **110,** 298–310.

Keller, E.A., Gurrola, L. & Tierney, T.E., 1999. Geomorphic criteria to determine direction of lateral propagation of reverse faulting and folding, *Geology,* **27,** 515–518.

Lawrence, R.D., Khan, S.H. & Nakata, T., 1992. Chaman Fault, Pakistan-Afghanistan, in *Major Active Faults of the World. Results of IGCP Project 206,* eds Buckham, R.C. & Hancock, P.L., *Ann. Tect., Spec. Issue,* supplement to **6,** 196–223.

Lettis, W.R., Wells, D.L. & Baldwin, J.N., 1997. Empirical observations regarding reverse earthquakes, blind thrust faults, and Quaternary deformation: are blind thrusts truly blind?, *Bull. seism. Soc. Am.,* **87,** 1171–1198.

Luyendyk, B.P., Kammerling, M.J. & Terres, R.R., 1980. Geometric model for Neogene crustal rotations in southern California, *Geol. Soc. Am. Bull.,* **91,** 211–217.

Matheson, S.A., 1976. *Persia: An Archaeological Guide,* 2nd edn, Faber & Faber, London.

McCaffrey, R. & Abers, G., 1988. SYN3: a program for inversion of teleseismic body waveforms on microcomputers, *Air Force Geophys. Lab. Tech. Rept,* **AFGL-TR-88-0099,** Hanscomb Air Force Base, MA.

McCaffrey, R. & Nabelek, J., 1987. Earthquakes, gravity and the origin of the Bali basin: an example of a nascent continental fold-and-thrust belt, *J. geophys. Res.,* **92,** 441–460.

McCaffrey, R., Zwick, P. & Abers, G., 1991. SYN4 Program, *IASPEI Software Library,* **3,** 81–166.

Meyer, B., Tapponnier, P., Bourjot, L., Metivier, F., Gaudemer, Y., Peltzer, G., Shunmin, G. & Zhitai, C., 1998. Crustal thickening in Gansu-Qinghai, lithospheric mantle subduction, and oblique, strike-slip controlled growth of the Tibet plateau, *Geophys. J. Int.,* **135,** 1–47.

Miller, D.D., 1998. Distributed shear, rotation, and partitioned strain along the San Andreas fault, central California, *Geology,* **26,** 867–870.

Molnar, P. & Gipson, J.M., 1994. Very long baseline interferometry and active rotations of crustal blocks in the Western Transverse Ranges, California, *Geol. Soc. Am. Bull.,* **106,** 594–606.

Molnar, P. & Lyon-Caen, H., 1989. Fault plane solutions of earthquakes and active tectonics of the Tibetan Plateau and its margin, *Geophys. J. Int.,* **99,** 123–153.

Mount, V.S. & Suppe, J., 1987. State of stress near the San Andreas Fault: implications for wrench tectonics, *Geology,* **15,** 1143–1146.

Nabelek, J., 1984. Determination of earthquake source parameters from inversion of body waves, *PhD thesis,* MIT.

Namson, J. & Davis, T., 1988. Structural transect of the western Transverse Ranges, California: implications for lithospheric kinematics and seismic risk evaluation, *Geology,* **16,** 675–679.

Philip, H., Rogozhin, E., Cisternas, A., Bousquet, J.C., Borisov, B. & Karakhanian, A., 1992. The Armenian earthquake of 1988 December 7: faulting and folding, neotectonics and palaeoseismicity, *Geophys. J. Int.,* **110,** 141–158.

Savage, J.C. & Hastie, L.M., 1966. Surface deformation associated with dip-slip faulting, *J. geophys. Res.,* **71,** 4897–4904.

Scholz, C.H., Aviles, C. & Wesnousky, S., 1986. Scaling differences between large intraplate and interplate earthquakes, *Bull. seism. Soc. Am.,* **76,** 65–70.

Shaw, J.H. & Suppe, J., 1994. Active faulting and growth folding in the eastern Santa Barbara channel, California, *Geol. Soc. Am. Bull.,* **106,** 607–626.

Taymaz, T., Jackson, J. & McKenzie, D., 1991. Active tectonics of the north and central Aegean Sea, *Geophys. J. Int.,* **106,** 433–490.

Tirrul, R., Bell, I.R., Griffis, R.J. & Camp, V.E., 1983. The Sistan suture zone of eastern Iran, *Geol. Soc. Am. Bull.,* **94,** 134–150.

Wessel, P. & Smith, W.H.F., 1995. New version of the Generic Mapping Tools released, *EOS, Trans. Am. geophys. Un.,* **76,** 329.

White, N.J., Jackson, J.A. & McKenzie, D.P., 1986. The relationship between the geometry of normal faults and that of the sedimentary layers in their hanging walls, *J. struct. Geol.,* **8,** 897–909.

Yeats, R.S., 1993. Tectonics: converging more slowly, *Nature,* **366,** 299–301.

Yeats, R.S., Sieh, K. & Allen, C.R., 1997. *The Geology of Earthquakes,* Cambridge University Press, Cambridge.

Yielding, G., Jackson, J.A., King, G.C., Sinhval, H., Vita-Finzi, C. & Wood, R.M., 1981. Relations between surface deformation, fault geometry, seismicity and rupture characteristics during the El Asnam (Algeria) earthquake of 10 October 1980, *Earth planet. Sci. Lett.,* **56,** 287–304.

Zwick, P., McCaffrey, R. & Abers, G., 1995. MT5 Program, *IASPEI Software Library,* **4**.

APPENDIX A: ENGINEERING ASPECTS AND STRONG GROUND MOTION

The damage caused by the 1994 earthquakes was typical for events of this size in eastern Iran. Traditional rural houses, with sun-dried mud-brick walls and roofs of mud domes or wooden poles, collapsed or were heavily damaged. Masonry buildings with brick walls reinforced by vertical and horizontal concrete tie beams, such as the Sefidabeh primary and secondary schools, and the Sefidabeh telecommunication station (on the ridge 2 km NW of Sefidabeh), suffered only minor damage. Three spans of the 192-m-long bridge across the Rud-e-Butgow 5 km N of Sefidabeh were displaced and damaged. At the telecommunication station a microwave rack was damaged and a water tank toppled.

The earthquake sequence triggered numerous rockfalls along steep mountain slopes damaging secondary roads, especially to the telecommunication station and along Palang Kuh (*lit*. 'tiger mountain') S and SW of Sefidabeh (Fig. 4b). Spring water flow at Sefidabeh increased after the first main shock.

The first large event of 23 February triggered the SMA-1 strong-motion instrument at Neh, 80 km NW of Sefidabeh, which recorded 0.019*g* maximum acceleration (Building and Housing Research Center 1994). The instruments at Zabol (92 km to the east) and Zahedan (170 km to the south) were not triggered. Temporary SSA-2 and SMA-1 accelerographs were installed locally to record aftershocks (Building and Housing Research Center 1994).